Biophysical Journal
Article

Biophysical Society

Transition from Actin-Driven to Water-Driven Cell Migration Depends on External Hydraulic Resistance

Yizeng Li[1] and Sean X. Sun[1,2,3,*]
[1]Department of Mechanical Engineering, [2]Johns Hopkins Institute for NanoBioTechnology, and [3]Johns Hopkins Physical Sciences-Oncology Center, Johns Hopkins University, Baltimore, Maryland

ABSTRACT Cells in vivo can reside in diverse physical and biochemical environments. For example, epithelial cells typically live in a two-dimensional (2D) environment, whereas metastatic cancer cells can move through dense three-dimensional matrices. These distinct environments impose different kinds of mechanical forces on cells and thus potentially can influence the mechanism of cell migration. For example, cell movement on 2D flat surfaces is mostly driven by forces from focal adhesion and actin polymerization, whereas in confined geometries, it can be driven by water permeation. In this work, we utilize a two-phase model of the cellular cytoplasm in which the mechanics of the cytosol and the F-actin network are treated on an equal footing. Using conservation laws and simple force balance considerations, we are able to describe the contributions of water flux, actin polymerization and flow, and focal adhesions to cell migration both on 2D surfaces and in confined spaces. The theory shows how cell migration can seamlessly transition from a focal adhesion- and actin-based mechanism on 2D surfaces to a water-based mechanism in confined geometries.

INTRODUCTION

Animal cell migration is a complex process orchestrated by actin dynamics, focal adhesions, and also water flux (1,2). However, how these elements are added together to obtain the observed cell speed is less clear. For example, cell migration on two-dimensional (2D) surfaces is mostly driven by forces from actin polymerization and focal adhesions (3), and there has been extensive work on modeling actin-driven cell migration on 2D surfaces (4–6), whereas cells in confined geometries can be driven by water permeation (7). Moreover, cells in confined channels show a diversity of behavior: some cells such as MDA-MB-231 (human breast cancer cell line) show reduced migration speed when actin is disrupted (8,9), whereas for others such as S180 (mouse sarcoma cell line), the migration speed is unaffected (7). In addition to varying responses to actin inhibition, cell movement in confinement appears to be sensitive to hydraulic resistance (10). Even more complex are cells in three-dimensional (3D) collagen matrices, where they develop long protrusions that interact with the collagen fibers, pores, and interstitial fluid (11–15). Depending on the cell shape, the nucleus may also play a significant role in propelling the cell (16). Thus, there are diverse mechanisms driving cell migration (17). We would like to understand whether there are unified physical principles and mechanisms giving rise to the wide range of observed cell behavior. Can we explain the impact of the physical environment on the speed of cell migration? In this work, by focusing on the combined contributions from actin dynamics and water flow, we develop a general model to understand mechanisms of cell migration in 3D, 2D, and one-dimensional (1D) environments (Fig. 1, *A–C*). In all these cases, we examine an effective one-dimensional volume element of a cell and compute the leading-edge cell speed for different actin- and water-flow dynamics. We find that the hydraulic environment of the cell potentially has a counterintuitive impact on the cell speed and determines the contribution of actin and water to the observed cell movement. In particular, cells can speed up if the coefficient of external hydraulic resistance increases, even when there is no change in the molecular elements driving migration. These results explain the diversity of observed cell-migration mechanisms and suggest that cells moving in 3D matrices are not only influenced by collagen fibers but also the hydrodynamic environment.

Submitted February 1, 2018, and accepted for publication April 27, 2018.
*Correspondence: ssun@jhu.edu
Editor: Celeste Nelson.
https://doi.org/10.1016/j.bpj.2018.04.045
© 2018 Biophysical Society.

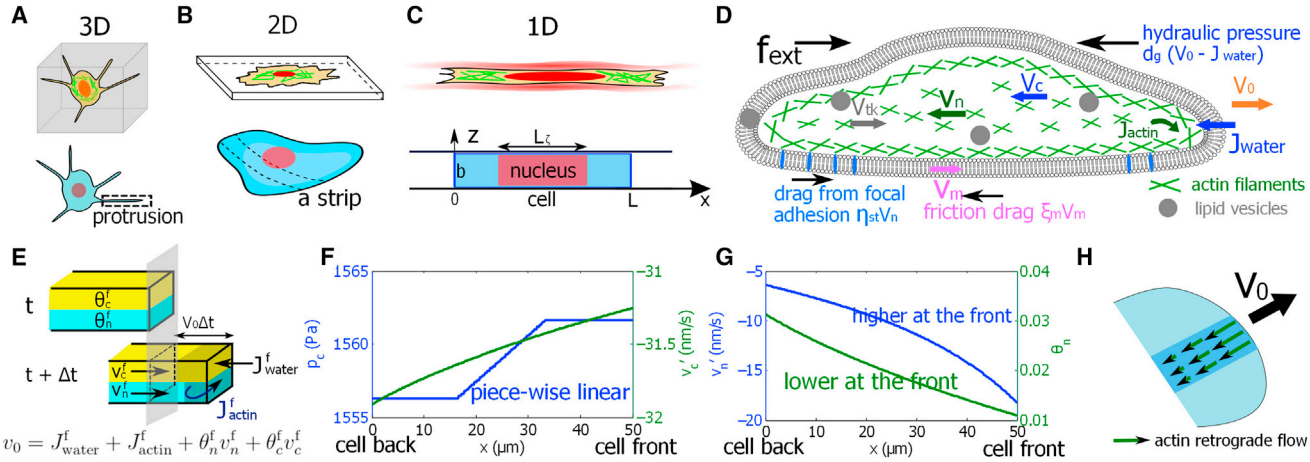

FIGURE 1 A two-fluid-phase cell-migration model. (*A*) The schematics of a cell in a 3D collagen gel are shown. The thin protrusion can be regarded as a 1D structure. (*B*) The schematics of a cell on a 2D substrate are shown. A strip of a cell on a 2D substrate can be regarded a 1D structure. (*C*) The schematics of a cell in a confined space are shown. In this case, the cell is essentially 1D. The model represents a cell (or a strip) with length L and width b. (*D*) A diagram of the relevant forces that contribute to cell migration is given. $v_{n,c}$ is the actin network and cytosol phase velocity, respectively. v_{tk} is the possible vesicle trafficking rate from the back to the front. The actin phase forms focal adhesion with the environment, resulting in a frictional drag force $\eta_{st}v_n$. Membrane movement also generates frictional force ($\xi_m v_m$). As the cell displaces external water, the hydraulic resistance can be expressed as $d_g(v_0 - J_{water})$, where v_0 is the cell boundary velocity. (*E*) A unit cross-sectional area of the cell leading edge is given. An exact kinematic relation for two-phase cell migration from time t to $t + \Delta t$ can be derived from mass balance. Each phase is attached to the cell leading edge (no void space) so that the cell velocity is related to the velocity of each phase. J^f_{actin} is the actin polymerization rate at the leading edge. J^f_{water} is the water influx rate at the leading edge. $\theta_{c,n}$ is the volume fraction of the cytosol actin network phase, respectively. v^f_c and v^f_n are the intracellular fluid velocities at the leading edge for the cytosol and actin phase, respectively. (*F*) The computed intracellular hydrostatic pressure field (*left axis*) and cytosol velocity field with respect to the cell frame (*right axis*) are shown. $v'_c = v_c - v_0$. (*G*) The computed intracellular actin velocity field with respect to the cell frame (*left axis*) and its volume fraction (*right axis*) are shown. $v'_n = v_n - v_0$. (*H*) A diagram of the actin retrograde flow predicted by the model is given. To see this figure in color, go online.

MATERIALS AND METHODS

A two-phase model of cell migration

To avoid complications associated with cell geometry, in this work, we mainly discuss a 1D-volume element of a moving cell. For example, for cells in 3D collagen matrices (Fig. 1 *A*), the thin protrusions can be regarded as 1D structures. For cells on 2D substrates (Fig. 1 *B*), we model a 1D strip of the cell. In this case, we only consider velocities and forces perpendicular to the cell leading edge. The effect of external bulk fluid flow in 2D is not considered in the model. For cells in a confined space (Fig. 1 *C*), the actin network and water flows can be directly modeled in 1D. In this case, the cell nucleus provides additional drag forces on the cytoplasm as the flows pass around or through (for the water phase) the nucleus. Within the 1D framework, the cell boundary is reduced to a front ("f") and a back ("b"). We use superscripts "f" and "b" to denote quantities associated with the cell front (leading edge) and back (trailing edge), respectively. In the following, we discuss briefly the 1D two-phase model of cell migration; more details and explanations can be found in the Supporting Materials and Methods.

In our model, we treat the cytosol (c, which is essentially water) and the actin network (n) as two fluid phases interacting with each other (18) and with the environment. The essential elements in the model are illustrated in Fig. 1 *D*. The volume fraction and velocity of the cytosol (actin network) phase are $\theta_c(\theta_n)$ and $v_c(v_n)$, respectively. In the frame of the cell body when the flow is steady, mass conservation conditions of the two phases are

$$\frac{d}{dx}\left[\theta_n v'_n\right] = 0 \tag{1}$$

and

$$\frac{d}{dx}\left[\theta_c v'_c\right] = 0, \tag{2}$$

where $v'_n = v_n - v_0$ and $v'_c = v_c - v_0$ are the velocities of the two phases in the frame of the moving cell and v_0 is the steady migration velocity of the leading edge and the cell.

For moving cells, new actin filaments are polymerized at the cell boundary with a rate $J^{f/b}_{actin}$. Similarly, water influx, $J^{f/b}_{water}$, also occurs at the cell boundary. In this model, $J^{f/b}_{actin}$ is a parameter, and $J^{f/b}_{water}$ is calculated from the chemical potential difference of water, i.e., $J^{f/b}_{water} = -\alpha^{f/b}(\Delta P^{f/b} - \Delta\Pi^{f/b})$, where $\Delta P^{f/b}$ and $\Delta\Pi^{f/b}$ are, respectively, the hydrostatic and osmotic pressure differences across the cell membrane and $\alpha^{f/b}$ is a coefficient of membrane water permeability. The cell can control $\Delta\Pi^{f/b}$ by generating ion fluxes at the cell boundary, and therefore we take it as a parameter. $\Delta P^{f/b}$ must be computed from mechanical considerations.

Because there are no void spaces, the cell boundary velocity is closely related to the boundary velocity of each phase. At the leading edge of the cell, as illustrated in Fig. 1 *E*, boundary kinematic relations read as $\theta^f_c v^f_c + J^f_{water} = v_0\theta^f_c$ and $\theta^f_n v^f_n + J^f_{actin} = v_0\theta^f_n$. Therefore, the velocity of the cell boundary is

$$v_0 = J^f_{water} + J^f_{actin} + \theta^f_n v^f_n + \theta^f_c v^f_c, \tag{3}$$

where we have used $\theta_c + \theta_n = 1$. Eq. 3 suggests that both water flux and actin polymerization can potentially contribute to cell migration (19). In a steady state with constant cell volume, $J^f_{actin} = -J^b_{actin}$ and $J^f_{water} = -J^b_{water}$; we thus use the notations $J_{actin} = J^f_{actin}$ and $J_{water} = J^f_{water}$ to represent the magnitude of these fluxes in the cell.

During cell migration, the cell membrane has a translational velocity, v_m, with respect to the surroundings. This motion leads to a frictional force between the cell and the surroundings. This force can be expressed as $f_m = -\xi_m v_m$, where ξ_m is the coefficient of frictional drag. v_m and v_0 are typically equivalent, but they can also be different if we include the velocity of membrane growth or extension from vesicle trafficking (20), v_{tk}. In this case, the apparent velocity of the cell boundary, v_0, is

formally a sum of the translational velocity of the lipid membrane and the velocity from vesicle trafficking, i.e., $v_0 = v_m + v_{tk}$. v_{tk} depends on the cell membrane tension, τ (21,22). Note that vesicle trafficking does not affect Eq. 3, which is only based on the assumption that the actin network phase is always attached to the membrane. This assumption holds during typical tissue-cell migration. One violation of such a condition is blebbing motility (23), in which the membrane extends without actin. Although blebbing motility can be analyzed within the two-phase framework, the details are more complicated. We will not discuss this case here.

If we regard the actin network as isotropic, it then also has an effective pressure that is different from the cytosol phase because of active contractions from myosin. The actin network is linked to the underlying substrate through focal adhesions and integrins (24). As the actin network flows, this linkage transmits a force from the environment to the actin network and thus onto the entire cell. For low actin-flow velocities, the force from focal adhesions is approximately proportional to the velocity of actin flow (25), i.e., $f_{st} = -\eta_{st} v_n$, where η_{st} is the coefficient of focal adhesion friction. Factors that can influence η_{st} include the substrate stiffness (26,27) and the size (28) and density (29) of adhesions. In this work, we restrict ourselves to understanding the mechanism of cell migration for a linear force-velocity relation for the focal adhesions. Experiments (25) and theory (27,30,31) have shown that the adhesion force-velocity relationship is generally complex and nonlinear. This can be incorporated into our model, but the details are not analyzed here.

To predict the cell velocity from Eq. 3, we need to know intracellular velocities v_n^f and v_c^f. These must be solved from mechanical force balance. When all of the forces are considered, the conservation of momentum for the two cytoplasmic fluid phases are

$$0 = -\theta_c \frac{d}{dx} P_c + \eta \theta_n \theta_c \left(v_n' - v_c'\right) - \zeta_c \theta_c v_c' \tag{4}$$

and

$$0 = -\theta_n \frac{d}{dx} P_c - \eta_n \theta_n \left[v_n' + (v_0 - v_m)\right] + \eta \theta_n \theta_c \left(v_c' - v_n'\right)$$

$$-\frac{d}{dx}(\theta_n \phi_n) - \eta_{st} \theta_n \left(v_n' + v_0\right) - \zeta_n \theta_n v_n', \tag{5}$$

where η is the coefficient of interphase viscous drag, η_n is the effective viscosity of the actin phase, and $\zeta_c(x)$ and $\zeta_n(x)$ are the coefficients of frictional drag from the nucleus on the cytosol and on the actin phases, respectively; these are only defined in the region where the nucleus is present. P_c and $P_n = P_c + \phi_n$ are the cytosol and network phase pressures, respectively. We write the excess pressure in the network phase as $\theta_n \phi_n$, which is also related to active contraction generated by myosin.

As the cell boundary moves at velocity v_0, the cell may experience an extracellular hydraulic resistance (in units of pressure, because this force is exerted on an area element). When $v_0 \neq J_{water}$, the cell boundary must push the external fluid at velocity $v_* = v_0 - J_{water}$. In the extreme case of a cell in a confined channel, the cell must push the complete column of water in front of the cell at the velocity v_*, and the friction between the extracellular fluid and the channel wall generates a large hydraulic resistance. This hydraulic resistance can be expressed as a linear function of v_*, i.e., $P_* = d_g(v_0 - J_{water})$, where d_g is a coefficient to be determined by the extracellular geometry and flow properties. In addition, the cell may experience external forces from extracellular objects such as mounted cantilever (32). We use f_{ext} to account for this effective force per unit area (again in units of pressure). Therefore, the force balance of the cell membrane is

$$b\left[\left(P_{in}^f - P_*^f\right) - \left(P_{in}^b - P_*^b\right)\right] + b f_{ext}^f - b f_{ext}^b = -b\eta_n \int_0^L \theta_n \left[v_n' + (v_0 - v_m)\right] dx + 2\xi_m v_m L. \tag{6}$$

The cell boundary velocity v_0 can be solved by integrating the sum of Eqs. 4 and 5 and adding that to Eq. 6. In the limit of $v_m = v_0$, v_0 can be solved analytically as follows (see Supporting Materials and Methods for more information):

$$v_0 = \frac{L\eta_{st} J_{actin} + f_{ext}^f - f_{ext}^b}{L\eta_{st}\Theta_n + 2\xi_m L/b + d_g} + \frac{L_\zeta(\zeta_c J_{water} + \zeta_n J_{actin}) + d_g J_{water}}{L\eta_{st}\Theta_n + 2\xi_m L/b + d_g}, \tag{7}$$

where L and b are the length and width of the cell (or a strip of cell), respectively, L_ζ is the length of the nucleus (Fig. 1 *C*), and Θ_n is the average volume fraction of the actin phase, satisfying $\int_0^L \theta_n(x)dx = L\Theta_n$. The approximation $v_m = v_0$ is valid when the net flux of vesicle trafficking is negligible. This can occur when the membrane-tension gradient across the cell is negligible or when the rate of vesicle formation is low. We will show that the membrane-tension gradient is indeed very small for the underlying physics included in the model. In this work, we also have not considered membrane blebbing and thus also neglect any membrane-tension changes due to blebbing (33).

The numerical values of parameters for the model are listed in Table 1. Unless otherwise specified or varied, these parameters are used throughout the work. More details on the physical interpretation of each parameter can be found in the Supporting Materials and Methods.

RESULTS AND DISCUSSION

The nucleus can increase the intracellular pressure difference

Fig. 1, *F* and *G* show a typical distribution of the intracellular hydrostatic pressure, volume fraction of the actin phase, and velocities of the two phases for a migrating cell with respect to the cell moving frame (see Supporting Materials and Methods for parameters). The velocity of the cell edge and the membrane translation are predicted to be the same, $v_0 = v_m = 12$ nm/s. Therefore, in this case, vesicle trafficking has a negligible effect. This is because the membrane tension difference between the cell front and back is negligible (see Supporting Materials and Methods and a later section). For the assumed osmotic pressure gradient, the water flux into the cell at the front is $J_{water} = 31$ nm/s, whereas the actual cell velocity is much smaller. Because $v_0 \neq J_{water}$, the cell displaces the extracellular fluid as it migrates.

The average intracellular hydrostatic pressure, P_c, is determined by the average osmolarity difference across the cell. In confined channels, the nucleus also influences P_c, giving rise to a piece-wise linear pressure profile. Larger effective drag from the nucleus on the cytosol, i.e., larger ζ_c, induces higher pressure difference between the front and back of the cell. When $\zeta_c = 0$, then P_c is a smooth function over the entire cell length, and the difference of P_c across the

TABLE 1 Parameters Used in the Models

Parameters	Description	Values	Sources
R (J/mol K)	ideal gas constant	8.31451	constant
T (K)	absolute temperature	300	room temperature
L (μm)	cell length	50	generic
L_ζ (μm)	nucleus length	$L/2$	generic
b (μm)	cell width	3	generic
h (μm)	membrane thickness	0.5	(48)
η (Pa • s/μm^2)	drag coefficient between two phases	1	(49)
η_n (Pa • s/μm^2)	effective viscosity in the actin phase	1.3	see text
ζ_c (Pa • s/μm^2)	effective drag coefficient from the nucleus to the cytosol phase	10	assumed
ζ_n (Pa • s/μm^2)	effective drag coefficient from the nucleus to the actin network phase	100	assumed
ξ_m (Pa • s/μm)	coefficient of friction of the channel wall	1	(7)
η_{st} (Pa • s/μm^2)	coefficient of drag from focal adhesion	1×10^4	(25)
d_g (Pa • s/μm)	coefficient of hydraulic pressure	1×10^3	see text
f_{ext}^f (Pa)	external force per unit area at the front	0	generic
f_{ext}^b (Pa)	external force per unit area at the back	0	generic
α^f (μm/(Pa • s))	water permeability constant at the front	1.0×10^{-4}	(7)
α^b (μm/(Pa • s))	water permeability constant at the back	1.0×10^{-4}	(7)
γ_{tk}^0 (nm/s)	maximal rate of vesicle trafficking	10	assumed
τ_{max} (Pa m)	maximal membrane tension when vesicle trafficking stops	5×10^{-2}	assumed
Θ_n	average volume fraction of the actin phase	0.02	(50)
ϕ_n (Pa)	excess pressure in the actin network	-1000 (back) to -5000 (front)	assumed
J_{actin} (nm/s)	actin flux at the two boundaries	$10\Theta_n$	assumed
P_0^f (Pa)	extracellular hydrostatic pressure at the front	0	generic
P_0^b (Pa)	extracellular hydrostatic pressure at the back	0	generic
c_0^f (mM)	extracellular ion concentration at the front	340	(7)
c_0^b (mM)	extracellular ion concentration at the back	340	(7)
c_{in}^f (mM)	intracellular ion concentration at the front	340.75	generic
c_{in}^b (mM)	intracellular ion concentration at the back	340.5	generic

These are the default parameters unless otherwise specified.

cell is reduced (see Fig. S2). This result is consistent with the "nuclear piston" mode of migration, in which the pressure gradient of the nucleus can influence cell speed (16). With the nucleus, the model predicts the same average intracellular cytosol pressure as the case without the nucleus; only $\Delta P_c = P_c^f - P_c^b$ is different. The relative velocity of the cytosol, $v_c' = v_c - v_0$ (shown in Fig. 1 *F*), is determined mostly by the boundary condition, i.e., $v_c'(L) = -J_{water}/\theta_c(L)$. Higher $|v_c'|$ at the back of the cell is consistent with the lower cytosolic volume fraction, because the product $\theta_c v_c'$ must be a constant from the mass conservation.

Retrograde flow is prominent at the cell leading edge

The relative velocity of the actin network, $v_n' = v_n - v_0$ (shown in Fig. 1 *G*), is largely determined by the rate of actin (de)polymerization at the boundaries, i.e., $v_n'(L) = -J_{actin}/\theta_n(L)$. In this example, the actin velocity at the cell front in the fixed frame is $v_n^f = v_n'^f + v_0 = -6$ nm/s. This negative velocity pointing inwards is the actin retrograde-flow motion commonly seem during cell migration (34). Our model also predicts a decrease of the retrograde velocity toward the back of the cell (Fig. 1 *G*) as seen in experiments (35). A cartoon depiction of actin retrograde flow is shown in Fig. 1 *H*. Because of the boundary condition specified in the model, we do not consider an anterograde actin flow at the back of the cell (6).

Cell migration on 2D substrates relies on actin dynamics and focal adhesion

For cells on 2D substrates, the coefficient of hydraulic resistance is negligible ($d_g^{2D} = 0$; see the Supporting Materials and Methods for more information), and the effective drag from the nucleus on the two phases can be neglected as well ($\zeta_c = \zeta_n = 0$). Hence, Eq. 7 is reduced to a simpler form in which v_0 is independent of J_{water}. The model predicts that v_0 scales with the rate of actin polymerization, J_{actin}/Θ_n, and the coefficient of focal adhesions, η_{st} (Fig. 2 *A*). In the limit of large η_{st} (for example, along the line $\eta_{st} = 10^4$ Pa • s/μm^2), the effect of ξ_m and $f_{ext}^{f/b}$ diminishes and $v_0 \simeq J_{actin}/\Theta_n$, suggesting that when the strength of focal adhesion is high (no slip), the cell velocity is determined by the rate of actin polymerization. On the other hand, when the force from focal adhesions is abolished (along the line $\eta_{st} = 1$ Pa • s/μm^2), v_0 does not increase as J_{actin} increases. This is consistent with the finding that for actin polymerization to be effective, there must be sufficient focal adhesion friction (24).

Fig. 2 *B* shows the predicted relation between v_0 and actin retrograde velocity as J_{actin} varies for different η_{st}. A higher

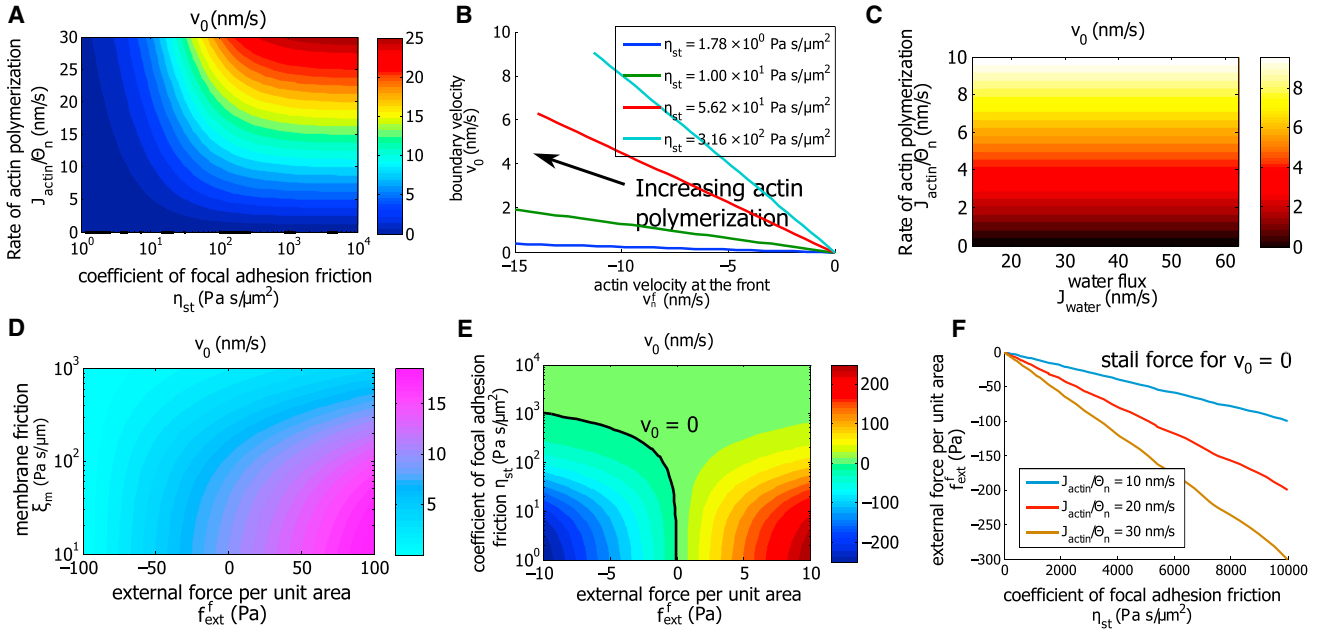

FIGURE 2 Cell migration on 2D substrates. (*A*) The contours of the cell boundary velocity, v_0, are shown as functions of actin polymerization rate J_{actin} and focal adhesion friction coefficient η_{st}. $J_{\text{actin}}/\Theta_n$ is a measure of actin velocity at the cell boundary generated by actin polymerization. In the calculation, J_{actin} varies and Θ_n remains unchanged. (*B*) The cell boundary velocity v_0 is given as a function of v_n^{f} for different coefficient of focal adhesion η_{st}. (*C*) The contours of v_0 as J_{actin} and J_{water} vary as shown. In 2D, J_{water} does not influence cell boundary velocity. (*D*) The contours of v_0 as ξ_m and $f_{\text{ext}}^{\text{f}}$ vary as shown. (*E*) The contours of v_0 as $f_{\text{ext}}^{\text{f}}$ and η_{st} vary as shown. (*F*) The stall force per unit area for different η_{st} is given. As expected, the magnitude of the stall force increases with increasing coefficients of focal adhesion friction or the rate of actin polymerization. To see this figure in color, go online.

rate of actin polymerization results in a higher cell velocity and also a higher magnitude of actin retrograde flow, because $\left|v_n^{\text{f}}\right|$ increases faster than v_0. For the same actin velocity v_n, the model predicts a higher v_0 for higher η_{st}.

Although the cell boundary velocity is in general influenced by the water flux through the membrane (Eq. 3), the model predicts that under negligible hydraulic resistance ($d_g^{\text{2D}} = 0$), the boundary velocity is independent of J_{water}. This can also be seen from Eq. 7, in which J_{water} does not contribute to v_0 when $d_g = 0$. More discussion is given in a later section.

Influence of external force on cell migration

The cell boundary moves faster if the membrane friction with the environment, $\xi_m v_m$, is low or the combination of the external forces (per unit area), $f_{\text{ext}}^{\text{f}} - f_{\text{ext}}^{\text{b}}$, points in the direction of cell migration (Fig. 2 *D*). Contour plots of v_0 as a function of η_{st} and $f_{\text{ext}}^{\text{f}}$ show a similar story (Fig. 2 *E*). We predict that when the friction force from focal adhesion is small (low η_{st}), v_0 scales linearly with $f_{\text{ext}}^{\text{f}}$; when the force from focal adhesion is large (high η_{st}), then the external forces have a negligible effect on cell velocity. Therefore, Fig. 2 *E* also implies an external force-cell velocity relation for cell migration. Similar calculations can be obtained for different rates of actin polymerization. We can extract the stall force when $v_0 = 0$ for each η_{st} and J_{actin}. As expected, the magnitude of the stall force increases as η_{st} or J_{actin} increases (Fig. 2 *F*). For a 2D cell's boundary element of 3 μm width and 200 nm height, the predicted stall force is on the order of 1 nN, which is of the same order as the stall force for cell boundary lamellipodium (32).

The spatial variation of the cell-membrane tension is set partially by the membrane friction with the environment and partially by the external force: larger ξ_m and $f_{\text{ext}}^{\text{f}} - f_{\text{ext}}^{\text{b}}$ can generate a membrane tension difference up to 10% from the back to the front of the cell (see Fig. S3). In other cases, the membrane tension is almost uniform across the cells, and thus the velocity contributed by the membrane trafficking is negligible. This result validates the assumption of $v_m = v_0$ that is used to approximate v_0 in Eq. 7. The viscosity of each phase or the friction between two phases has little contribution to v_0 (see Fig. S3), showing that for cells on 2D substrates, migration is mostly driven by actin polymerization, focal adhesion, and external forces acting on the cell.

Confined 1D cells migrate faster under higher coefficients of hydraulic resistance

For cells in confined channels (Fig. 3 *A*), the coefficient of hydraulic resistance is $d_g^{\text{1D}} = 12\mu_f \ell_0 / b^2$, where ℓ_0 is the total length of the channel and μ_f is the extracellular fluid viscosity in the channel (see the Supporting Materials and Methods for more information). A longer channel or a higher extracellular fluid viscosity leads to a higher

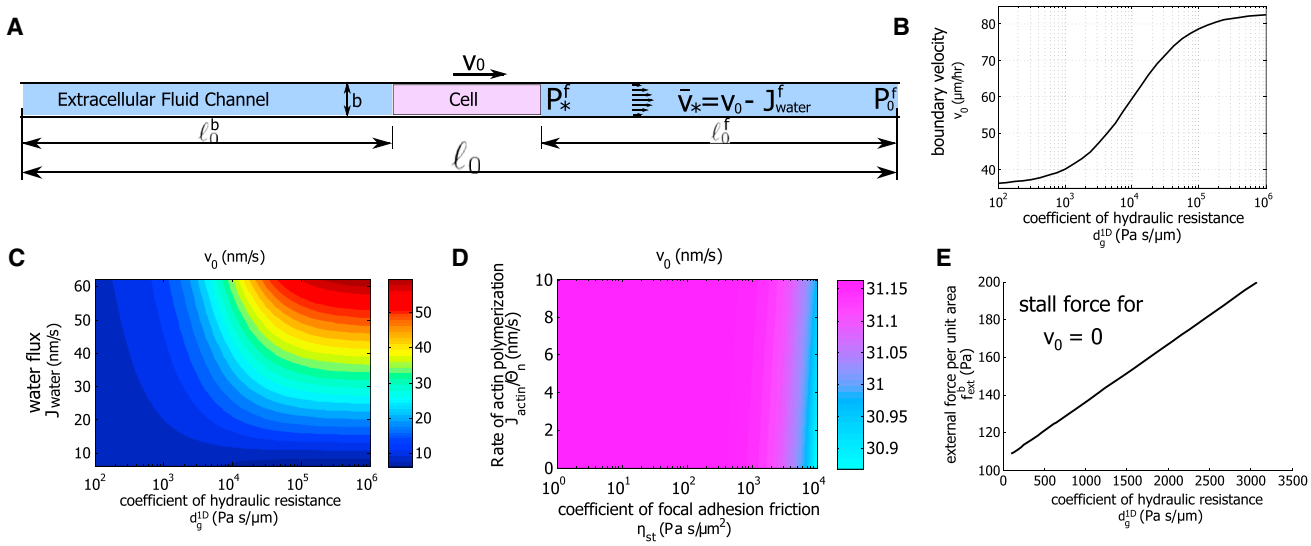

FIGURE 3 Confined 1D cells migrate faster under higher coefficients of hydraulic resistance. (*A*) A diagram of the cell and the external fluid flow in a 1D channel is shown. (*B*) A model prediction of the cell boundary velocity v_0 as d_g^{1D} varies is shown. Here, $c_{in}^f = 340.7$ mM, which corresponds to a water flux of $J_{water} = 82\ \mu$ m/h. (*C*) The velocity of the cell edge v_0 as J_{water} and d_g^{1D} vary as shown. We let c_{in}^f vary from 340.6 to 341 mM and obtain J_{water} accordingly. Cell velocity increases with increasing J_{water} and d_g^{1D}. (*D*) The contours of v_0 as J_{actin} and η_{st} vary as shown. Here, $d_g^{1D} = 10^6$ Pa•s/μm. For confined channels with high hydraulic resistance, neither actin polymerization nor focal adhesion friction influence the cell speed significantly. (*E*) Stall force per unit area increases with d_g^{1D}. To see this figure in color, go online.

coefficient of hydraulic resistance. In a typical channel in this work or in (7), for example, $b = 5\ \mu$ m, $\ell_0 = 500\ \mu$ m, and $\mu_f = 10^{-3}$ Pa • s, then d_g^{1D} is about 2.5×10^{-1} Pa • s/μm. In reality, d_g^{1D} can be much higher than this estimate because the channel walls are not smooth. Fig. 3 *B* shows the model prediction that v_0 increases with d_g^{1D} while the other parameters remain the same. The cell velocity saturates at low and high d_g^{1D}. For intermediate d_g^{1D}, one order of magnitude change of d_g^{1D}—for example, from 5×10^3 Pa • s/μm to 5×10^4 Pa • s/μm—results in an increase in cell velocity (from ~54 μm/h to ~75 μm/h) by ~40%.

This prediction, showing that cells move faster in an environment with a higher coefficient of hydraulic resistance, is rather counterintuitive. This result can be understood by considering the flow of the extracellular fluid. In Fig. 3 *B*, with constant J_{water}, v_0 increases as d_g^{1D} increases, meaning that the cell utilizes more of the water flux in v_0. This means the fluid velocity in the channel, $v_* = v_0 - J_{water}$, decreases with d_g^{1D}, which is expected under higher hydraulic resistance. In addition, the cytosol velocity v_c must be continuous with extracellular fluid velocity and decrease for larger d_g^{1D}. Therefore, the cell boundary velocity increases.

On the other hand, increased velocity of cell migration under a higher coefficient of hydraulic resistance, d_g^{1D}, helps to reduce the otherwise high hydraulic resistance, $d_g^{1D}v_*$: although the coefficient of hydraulic resistance varies from 10^2 to 10^6 Pa • s/μm, as shown in Fig. 3 *C*, the actual hydraulic resistance experienced by the cell remains in the same order of magnitude when the cell velocity v_0 increases (see Fig. S4). Note that in this work, we have assumed that the network phase is always attached to the cell boundary during continuous (de)polymerization, and the velocity of polymerization J_{actin} is constant. Experiments have shown that actin polymerization can adapt against mechanical resistance to grow at a constant velocity (36), which justifies this assumption, although, in principle, any dependence of J_{actin} on force can be incorporated in our model.

Transition between actin-driven and flow-driven cell migrations depends on the external coefficient of hydraulic resistance

Equation 3 suggests that v_0 increases with J_{water}; indeed, the model predicts that the cell migrates faster under larger water flux. Fig. 3 *C* shows the dependence of v_0 with J_{water} and d_g^{1D}. When d_g^{1D} is small ($d_g^{1D} < 10^2$ Pa • s/μm), the cell velocity is low and is almost independent of J_{water}, suggesting that water flux does not contribute to cell migration in this regime. This is the situation for cells on a 2D substrate (also see Fig. 2 *C*). When d_g^{1D} is large ($d_g^{1D} > 10^5$ Pa • s/μm), the cell velocity equals to J_{water}; this is the situation for a cell in a confined space where cell migration is mostly facilitated by water flux, i.e., an osmotic engine model (7). In this regime, the boundary velocity saturates with d_g^{1D}.

For a high coefficient of hydraulic resistance, for example, $d_g^{1D} = 10^6$ Pa • s/μm, the predicted cell velocity v_0 is independent of J_{actin} or η_{st} (Fig. 3 *D*). This result, together with Fig. 3 *C*, indicates that under a high coefficient of hydraulic resistance, v_0 is dominated by water flux, not the actin network, whereas under a low coefficient of hydraulic resistance, v_0 is dominated by the actin network, not water flux. Our model shows that the transition from

actin-driven cell migration to water-driven cell migration can result from the physical effects of fluid flow, not from a change in the mechanism of migration signaled by the cell.

Similar to the 2D case in which higher external forces are needed to stop cell migration under higher strength of focal adhesion (Fig. 2 *F*), in 1D, higher external forces are needed to stop cell migration under a higher coefficient of hydraulic resistance (Fig. 3 *E*). The magnitude of the stall force is therefore also a measure of the strength of the "driving force," which is focal adhesion and actin polymerization in 2D and water flux in 1D.

Hydraulic resistance in 3D matrices

The model can be extended to understand the influence of the hydraulic environment on cell migration in 3D matrices (hydrogels such as collagen) (Fig. 4 *A*). The front of the protrusion interacts with the matrix and the interstitial fluid. As the protrusion extends, it exerts a force on its environment and changes the hydrodynamic pressure distribution in the matrix. The extracellular matrix is a viscoelastic material with high porosity. The gel component, i.e., the collagen-fiber network, deforms as the cell protrudes and therefore exerts an external force on the migrating cell. In the case of collagen gels, the matrix is also disassembled as the cell migrates and secretes matrix metalloproteinases (37). We have seen in the previous sections that the coefficients of hydraulic resistance can vary significantly in 1D versus 2D. This difference can determine the relative contribution of different mechanisms of cell migration. In vivo, the mechanical properties of the collagen matrix are complex. Although much has been studied to understand the viscoelastic property and the porosity of the collagen matrix, it remains unclear what types of hydraulic resistance the cell experiences in 3D matrices and how this compares to the d_g in 1D and 2D. In this section, we explore how d_g in 3D depends on the mechanical properties of the collagen matrix.

Using a poroelastic theory, we estimate the effective coefficient of hydraulic resistance to be $d_g^{3D} = \mu_f b/2\kappa$ (see the Supporting Materials and Methods for more information), where μ_f is the effective viscosity of the fluid phase in the collagen matrix, κ is the permeability of the collagen matrix, and b is still the width of the cell protrusion. To differentiate the notation used in 1D, we will add "3D" or "1D" to the corresponding quantities in each geometry, i.e., $d_g^{3D} = \mu_f^{3D} b^{3D}/2\kappa$ and $d_g^{1D} = 12\mu_f^{1D}\ell_0/(b^{1D})^2$. We assume $\mu_f^{3D} = \mu_f^{1D}$. Depending on the values of $b^{3D}/2\kappa$ and $12\ell_0/(b^{1D})^2$, the coefficient of hydraulic resistance in 3D can be either larger or smaller than that in 1D. For example, when $\kappa = 10^{-16}$ m^2 (38), $b^{3D} = b^{1D} = 3$ μ m, and $\ell_0 = 10^3$ μm, then $d_g^{3D} > d_g^{1D}$. But when $\kappa = 10^{-12}$ m^2, then $d_g^{3D} < d_g^{1D}$. Fig. 4 *B* shows the phase diagram of the ratio $\ln(d_g^{1D}/d_g^{3D})$ as the 1D channel length ℓ_0 and the permeability of the collagen matrix κ vary. The line $\ln(d_g^{1D}/d_g^{3D}) = 0$ indicates $d_g^{1D} = d_g^{3D}$.

Depending on the viscosity of the interstitial fluid in the collagen matrix and the matrix hydraulic permeability, which is related to the collagen density, the coefficient of hydraulic resistance in 3D can be comparable to 1D (Fig. 4 *B*). This suggests that the hydraulic effects could play an important role in 3D cell protrusion, including morphogenesis and cancer cell metastasis. In experiments, it is found that cell velocity has a biphasic dependence on the collagen density (13), which may be attributed to collagen fiber alignment, matrix pore size (13), cell-matrix biochemical interaction, or the effect of the hydraulic resistance, which can occur when there is a large water flux through the cell surface and the hydraulic resistance starts to dominate at low matrix permeability. To fully study 3D cell migration, other matrix properties should be considered, including strain-stiffening (39), stress relaxation (40), collagen fiber alignment, matrix pore size, and production of matrix metalloproteinases (13). More extensive studies, both experimental and theoretical, are needed to address this complexity.

CONCLUSIONS

Understanding the mechanism of cell migration in different physical environments helps to uncover pathophysiological mechanisms. Using a two-phase modeling framework, we derived a general expression that is applicable to a wide range of physical conditions to compute the cell boundary velocity as a function of actin polymerization rate and water influx rate. The model incorporates

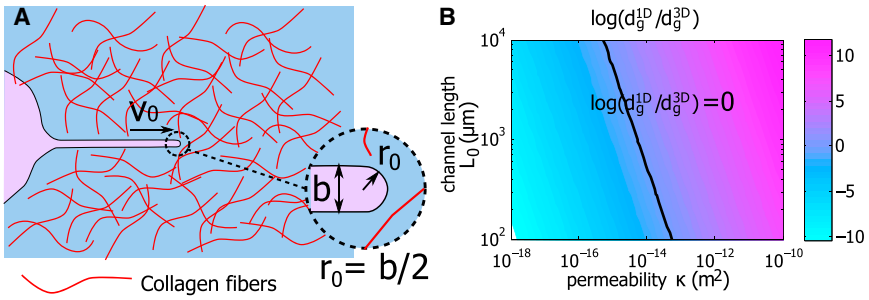

FIGURE 4 Cell movement in 3D collagen matrix. (*A*) A diagram of a cell protrusion and the surrounding collagen matrix is shown. Collagen fibers are distributed in the matrix. The tip of the protrusion has a radius $r_0 = b/2$, where b is the width of the protrusion. (*B*) The contour of $\ln(d_g^{1D}/d_g^{3D})$ as the 1D channel length ℓ_0 and the permeability of the collagen matrix κ vary is shown. The line is where $d_g^{1D} = d_g^{3D}$. To see this figure in color, go online.

known mechanics of important motility components and includes effects of focal adhesion and membrane friction force as well as hydraulic resistance from flow outside of the cell. Depending on the environmental properties, the coefficient of hydraulic resistance can be substantial, especially in 1D channels and 3D matrices. The coefficient of hydraulic resistance can influence the relative contribution of water influx to migration speed. In 2D environments, the hydraulic resistance is negligible so that even if the water influx is large, it does not contribute to cell speed as long as the cell maintains constant volume. In 1D confined channels with a high coefficient of hydraulic resistance, water influx enhances migration speed. In 3D matrices, the hydraulic resistance depends on the local environment of the cell and can be as large as the 1D case. This result suggests that in 3D, knocking out the cell components responsible for water flux would have major effects in cell motility.

In this work, we mainly focus on how cell migration may perturb the extracellular fluid environment and generate a hydraulic resistance back onto the cell; we have not considered bulk fluid flow from the environment, which can be relevant for cell migration on a 2D surface, e.g., endothelial cells in blood flow. When this bulk flow is in a confined geometry such as a blood vessel, we also expect a pressure drop in the flow and also across the cell. This hydrodynamic pressure difference across the cell can also influence cell migration. In unconfined geometries, the pressure drop across the cell is negligible during bulk flow. Instead, fluid shear stress on the cell surface is more important. This shear stress on the cell will activate membrane channels and further promote cell migration (41). A complete model incorporating effects from external bulk flow has not been developed.

Our results express the cell speed for given actin-polymerization and water-influx rates. However, exactly how these fluxes are controlled is not addressed and requires additional study and modeling. For example, the contraction of the actomyosin network is mediated by the strength of the focal adhesion. Biochemical feedback among the focal adhesion, actin flow, and actomyosin contraction can also generate traction oscillations within the adhesion (42,43). To resolve these effects, a more complicated model is needed to couple the contraction in the actomyosin network, actin flow, and the strength of adhesions. In addition, there is likely substantial cross talk between actin polymerization and water flux. Actin polymerization is linked to the polarity of the cell (44) and likely influences ion channels and pumps that set up the osmotic gradient (45). There are also direct interactions between ion channels and the cytoskeleton (46). Water and ion fluxes could also reorganize the cytoskeleton. This is especially true for calcium, which is implicated in activating myosin contraction (47). Therefore, examining the interplay between actin dynamics and water flux would yield new insights.

SUPPORTING MATERIAL

Supporting Materials and Methods and four figures are available at http://www.biophysj.org/biophysj/supplemental/S0006-3495(18)30567-8.

AUTHOR CONTRIBUTIONS

Y.L. and S.X.S. designed the theory and model, and Y.L. performed the calculations. Y.L. and S.X.S. wrote the manuscript.

ACKNOWLEDGMENTS

This work was supported by National Institutes of Health grants R01GM114675 and U54CA210172.

REFERENCES

1. Pollard, T. D., and G. G. Borisy. 2003. Cellular motility driven by assembly and disassembly of actin filaments. *Cell.* 112:453–465.
2. Tao, J., Y. Li, …, S. X. Sun. 2017. Cell mechanics: a dialogue. *Rep. Prog. Phys.* 80:036601.
3. Gardel, M. L., I. C. Schneider, …, C. M. Waterman. 2010. Mechanical integration of actin and adhesion dynamics in cell migration. *Annu. Rev. Cell Dev. Biol.* 26:315–333.
4. Barnhart, E. L., J. Allard, …, A. Mogilner. 2017. Adhesion-dependent wave generation in crawling cells. *Curr. Biol.* 27:27–38.
5. Craig, E. M., J. Stricker, …, A. Mogilner. 2015. Model for adhesion clutch explains biphasic relationship between actin flow and traction at the cell leading edge. *Phys. Biol.* 12:035002.
6. Shao, D., H. Levine, and W.-J. Rappel. 2012. Coupling actin flow, adhesion, and morphology in a computational cell motility model. *Proc. Natl. Acad. Sci. USA.* 109:6851–6856.
7. Stroka, K. M., H. Jiang, …, K. Konstantopoulos. 2014. Water permeation drives tumor cell migration in confined microenvironments. *Cell.* 157:611–623.
8. Poincloux, R., O. Collin, …, P. Chavrier. 2011. Contractility of the cell rear drives invasion of breast tumor cells in 3D Matrigel. *Proc. Natl. Acad. Sci. USA.* 108:1943–1948.
9. Carey, S. P., A. Rahman, …, C. A. Reinhart-King. 2015. Comparative mechanisms of cancer cell migration through 3D matrix and physiological microtracks. *Am. J. Physiol. Cell Physiol.* 308:C436–C447.
10. Prentice-Mott, H. V., C. H. Chang, …, J. V. Shah. 2013. Biased migration of confined neutrophil-like cells in asymmetric hydraulic environments. *Proc. Natl. Acad. Sci. USA.* 110:21006–21011.
11. Ahmadzadeh, H., M. R. Webster, …, V. B. Shenoy. 2017. Modeling the two-way feedback between contractility and matrix realignment reveals a nonlinear mode of cancer cell invasion. *Proc. Natl. Acad. Sci. USA.* 114:E1617–E1626.
12. Polacheck, W. J., A. E. German, …, R. D. Kamm. 2014. Mechanotransduction of fluid stresses governs 3D cell migration. *Proc. Natl. Acad. Sci. USA.* 111:2447–2452.
13. Fraley, S. I., P. H. Wu, …, D. Wirtz. 2015. Three-dimensional matrix fiber alignment modulates cell migration and MT1-MMP utility by spatially and temporally directing protrusions. *Sci. Rep.* 5:14580.
14. Doyle, A. D., N. Carvajal, …, K. M. Yamada. 2015. Local 3D matrix microenvironment regulates cell migration through spatiotemporal dynamics of contractility-dependent adhesions. *Nat. Commun.* 6:8720.
15. Petrie, R. J., and K. M. Yamada. 2016. Multiple mechanisms of 3D migration: the origins of plasticity. *Curr. Opin. Cell Biol.* 42:7–12.
16. Petrie, R. J., H. Koo, and K. M. Yamada. 2014. Generation of compartmentalized pressure by a nuclear piston governs cell motility in a 3D matrix. *Science.* 345:1062–1065.

17. Doyle, A. D., R. J. Petrie, …, K. M. Yamada. 2013. Dimensions in cell migration. *Curr. Opin. Cell Biol.* 25:642–649.
18. Cogan, N. G., and R. D. Guy. 2010. Multiphase flow models of biogels from crawling cells to bacterial biofilms. *HFSP J.* 4:11–25.
19. Hu, J., and A. S. Verkman. 2006. Increased migration and metastatic potential of tumor cells expressing aquaporin water channels. *FASEB J.* 20:1892–1894.
20. Fletcher, S. J., and J. Z. Rappoport. 2010. Moving forward: polarised trafficking in cell migration. *Trends Cell Biol.* 20:71–78.
21. Apodaca, G. 2002. Modulation of membrane traffic by mechanical stimuli. *Am. J. Physiol. Renal Physiol.* 282:F179–F190.
22. Diz-Muñoz, A., D. A. Fletcher, and O. D. Weiner. 2013. Use the force: membrane tension as an organizer of cell shape and motility. *Trends Cell Biol.* 23:47–53.
23. Fackler, O. T., and R. Grosse. 2008. Cell motility through plasma membrane blebbing. *J. Cell Biol.* 181:879–884.
24. Parsons, J. T., A. R. Horwitz, and M. A. Schwartz. 2010. Cell adhesion: integrating cytoskeletal dynamics and cellular tension. *Nat. Rev. Mol. Cell Biol.* 11:633–643.
25. Gardel, M. L., B. Sabass, …, C. M. Waterman. 2008. Traction stress in focal adhesions correlates biphasically with actin retrograde flow speed. *J. Cell Biol.* 183:999–1005.
26. Bangasser, B. L., G. A. Shamsan, …, D. J. Odde. 2017. Shifting the optimal stiffness for cell migration. *Nat. Commun.* 8:15313.
27. Walcott, S., and S. X. Sun. 2010. A mechanical model of actin stress fiber formation and substrate elasticity sensing in adherent cells. *Proc. Natl. Acad. Sci. USA.* 107:7757–7762.
28. Kim, D. H., and D. Wirtz. 2013. Focal adhesion size uniquely predicts cell migration. *FASEB J.* 27:1351–1361.
29. Cavalcanti-Adam, E. A., T. Volberg, …, J. P. Spatz. 2007. Cell spreading and focal adhesion dynamics are regulated by spacing of integrin ligands. *Biophys. J.* 92:2964–2974.
30. Harland, B., S. Walcott, and S. X. Sun. 2011. Adhesion dynamics and durotaxis in migrating cells. *Phys. Biol.* 8:015011.
31. Chan, C. E., and D. J. Odde. 2008. Traction dynamics of filopodia on compliant substrates. *Science.* 322:1687–1691.
32. Prass, M., K. Jacobson, …, M. Radmacher. 2006. Direct measurement of the lamellipodial protrusive force in a migrating cell. *J. Cell Biol.* 174:767–772.
33. Dai, J., and M. P. Sheetz. 1999. Membrane tether formation from blebbing cells. *Biophys. J.* 77:3363–3370.
34. Thievessen, I., P. M. Thompson, …, C. M. Waterman. 2013. Vinculin-actin interaction couples actin retrograde flow to focal adhesions, but is dispensable for focal adhesion growth. *J. Cell Biol.* 202:163–177.
35. Alexandrova, A. Y., K. Arnold, …, A. B. Verkhovsky. 2008. Comparative dynamics of retrograde actin flow and focal adhesions: formation of nascent adhesions triggers transition from fast to slow flow. *PLoS One.* 3:e3234.
36. Parekh, S. H., O. Chaudhuri, …, D. A. Fletcher. 2005. Loading history determines the velocity of actin-network growth. *Nat. Cell Biol.* 7:1219–1223.
37. Baker, B. M., and C. S. Chen. 2012. Deconstructing the third dimension: how 3D culture microenvironments alter cellular cues. *J. Cell Sci.* 125:3015–3024.
38. Vennat, E., D. Aubry, and M. Degrange. 2010. Collagen fiber network infiltration: permeability and capillary infiltration. *Transp. Porous Media.* 84:717–733.
39. Stein, A. M., D. A. Vader, …, L. M. Sander. 2011. The micromechanics of three-dimensional collagen-i gels. *Complexity.* 16:22–28.
40. Nam, S., K. H. Hu, …, O. Chaudhuri. 2016. Strain-enhanced stress relaxation impacts nonlinear elasticity in collagen gels. *Proc. Natl. Acad. Sci. USA.* 113:5492–5497.
41. Shiu, Y. T., S. Li, …, S. Chien. 2004. Rho mediates the shear-enhancement of endothelial cell migration and traction force generation. *Biophys. J.* 86:2558–2565.
42. Plotnikov, S. V., A. M. Pasapera, …, C. M. Waterman. 2012. Force fluctuations within focal adhesions mediate ECM-rigidity sensing to guide directed cell migration. *Cell.* 151:1513–1527.
43. Wu, Z., S. V. Plotnikov, …, J. Liu. 2017. Two distinct actin networks mediate traction oscillations to confer focal adhesion mechanosensing. *Biophys. J.* 112:780–794.
44. Lomakin, A. J., K. C. Lee, …, G. Danuser. 2015. Competition for actin between two distinct F-actin networks defines a bistable switch for cell polarization. *Nat. Cell Biol.* 17:1435–1445.
45. Rosado, J. A., S. Jenner, and S. O. Sage. 2000. A role for the actin cytoskeleton in the initiation and maintenance of store-mediated calcium entry in human platelets. Evidence for conformational coupling. *J. Biol. Chem.* 275:7527–7533.
46. Schwab, A., A. Fabian, …, C. Stock. 2012. Role of ion channels and transporters in cell migration. *Physiol. Rev.* 92:1865–1913.
47. Veksler, A., and N. S. Gov. 2009. Calcium-actin waves and oscillations of cellular membranes. *Biophys. J.* 97:1558–1568.
48. Jiang, H., and S. X. Sun. 2013. Cellular pressure and volume regulation and implications for cell mechanics. *Biophys. J.* 105:609–619.
49. Dembo, M., and F. Harlow. 1986. Cell motion, contractile networks, and the physics of interpenetrating reactive flow. *Biophys. J.* 50:109–121.
50. Satcher, R. L., Jr., and C. F. Dewey, Jr. 1996. Theoretical estimates of mechanical properties of the endothelial cell cytoskeleton. *Biophys. J.* 71:109–118.

Biophysical Journal, Volume *114*

Supplemental Information

Transition from Actin-Driven to Water-Driven Cell Migration Depends on External Hydraulic Resistance

Yizeng Li and Sean X. Sun

Supplementary Materials for Transition from actin-driven to water-driven cell migration depends on external hydraulic resistance

Y. Li and S.X. Sun

April 30, 2018

1 Mathematical Model

Let v_0 be the steady velocity of a 1D cell, the leading edge velocity of a 1D strip of a cell on a substrate, or a 1D protrusion of a cell in 3D collagen gel. For simplicity, we will just call the model a 1D cell, as illustrated in Fig. S1A. The cell has length L and all the variables only vary in the x direction. A nucleus of length L_ζ is at the middle of the cell. Two intracellular fluid phases, one for the cytosol (c) and one for the actin network (n), are modeled. We denote the volume fraction of the actin network and the cytosol as $\theta_n(x)$ and $\theta_c(x)$, respectively. The two volume fractions satisfy $\theta_n + \theta_c = 1$. The cytosol, which is mostly water, can have influx and efflux at the boundaries ($x = 0$ and $x = L$). The actin network is constrained within the cell and its average volume fraction, Θ_n, is constant under steady-state, i.e.,

$$\frac{1}{L}\int_0^L \theta_n(x)dx = \Theta_n\,. \tag{S1}$$

Without blebbing, each phase is effectively attached to the cell boundary (no void space) so that the boundary velocity is related to the velocity of each phase. At the front edge of the cell, as illustrated in Fig. S1B, the kinematic relations read as

$$\theta_c^{\mathrm{f}} v_c^{\mathrm{f}} + J_{\mathrm{water}}^{\mathrm{f}} = v_0\theta_c^{\mathrm{f}}\,, \tag{S2}$$

$$\theta_n^{\mathrm{f}} v_n^{\mathrm{f}} + J_{\mathrm{actin}}^{\mathrm{f}} = v_0\theta_n^{\mathrm{f}}\,, \tag{S3}$$

where the superscript 'f' indicates the front edge of the cell ($x = L$) and we will use the superscript 'b' to represent the back edge of the cell ($x = 0$). $v_n(x)$ and $v_c(x)$ are the velocities of the actin network and the cytosol, respectively, in a fixed frame (absolute velocities). Because of the lateral wall and cell membrane, v_c and v_n are functions in the cross-sectional directions as well; we incorporate this effect by taking v_c and v_n as the cross-sectional averaged velocities of the approximated quadratic profiles for the two

phases. Similarly, the shear stress present due to the quadratic velocity profiles are also implicitly included in the frictional force terms in the force balance equations below. J_{actin} in E. S3 is the given rate of actin (de)polymerization. In this model, we lump the effective actin (de)polymerization to the cell boundaries. It is possible to incorporate actin polymerization or depolymerization in the interior of the cell, and the results of cell migration velocity do not change qualitatively. Under steady-state conditions, $J^{\text{f}}_{\text{actin}} = -J^{\text{b}}_{\text{actin}} = J_{\text{actin}}$. J_{water} in Eq. S2 is the water flux across the cell boundary and satisfies

$$J^{\text{f}}_{\text{water}} = -J^{\text{b}}_{\text{water}} = J_{\text{water}} \tag{S4}$$

under steady-state. The combination of Eqs. S2 and S3 implies the velocity of the cell or cell boundary

$$v_0 = J^{\text{f}}_{\text{water}} + J^{\text{f}}_{\text{actin}} + \theta^{\text{f}}_n v^{\text{f}}_n + \theta^{\text{f}}_c v^{\text{f}}_c \,. \tag{S5}$$

Equation S5 suggests that both water flux and actin polymerization, in principle, can contribute to cell migration, i.e., the actual observed cell speed depends on the cytoplasmic velocity fields as well as boundary fluxes.

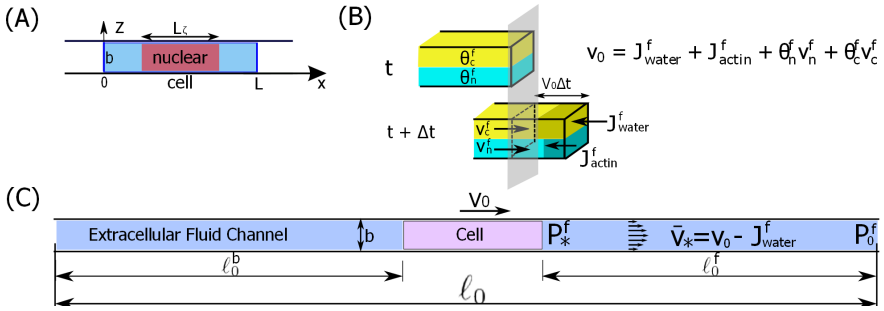

Figure S1: (A) Diagram of the coordinate system and dimension of the cell. (B) A unit cross-sectional area of the front leading edge. A generic kinematic relation for a two-phase cell migration from time t to $t + \Delta t$. Each phase is attached to the cell leading edge (no void space) so that the cell velocity is related to the velocity of each phase and its boundary condition. θ_c: volume fraction of the cytosol phase. θ_n: volume fraction of the actin network. (C) Diagram of the cell and the external fluid flow in a 1D channel.

We solve the system in the frame of the moving cell. The relative velocities of the two phases with respect to the cell are $v'_c = v_c - v_0$ and $v'_n = v_n - v_0$. In the frame of the cell body, Eqs. S2 and S3 becomes

$$\theta^{\text{f}}_c v'^{\text{f}}_c + J^{\text{f}}_{\text{water}} = 0 \,, \tag{S6}$$

and

$$\theta^{\text{f}}_n v'^{\text{f}}_n + J^{\text{f}}_{\text{actin}} = 0 \,, \tag{S7}$$

respectively. As long as Eqs. S6 and S7 are enforced, the relation for cell velocity in Eq. S5 is implied.

Water fluxes at the cell boundaries are proportional to the chemical potential difference of water across the membrane and is defined positive inward,

$$J^{\text{f/b}}_{\text{water}} = -\alpha^{\text{f/b}} \left[\left(P_c^{\text{f/b}} - P_*^{\text{f/b}} \right) - RT \left(c_{\text{in}}^{\text{f/b}} - c_0^{\text{f/b}} \right) \right] , \tag{S8}$$

where α is the coefficient of water permeability of the cell membrane, P_* is the extracellular hydrostatic pressure at the cell boundaries (see Fig. S1C), P_c is the hydrostatic pressure of the cytosol phase, and c_{in} and c_0 are the intracellular and extracellular ionic concentrations, respectively. In this work, without loss of generality, c_{in} and c_0 will be given; however, we can always extent the model to incorporate intracellular ion dynamics as been done in [1, 2].

The extracellular pressure at the front of the cell, P_*^{f}, can be different from the farfield pressure at the front of the channel, P_0^{f} (see Fig. S1B), if the moving cell generates extracellular fluid flow and pressure gradient. When the velocity of the cell boundary equals to the water flux across the cell membrane, i.e., $v_0 = J_{\text{water}}$, the cell does not push the external fluid so that all of the water flux contributes to v_0.; this is the case of an osmotic engine model [1, 2]. However, when $v_0 \neq J_{\text{water}}$, the cell pushes the external fluid and experiences hydraulic resistance from the extracellular environment; this force is proportional to $v_0 - J_{\text{water}}$. We can express P_*^{f} as

$$P_*^{\text{f}} = P_0^{\text{f}} + d_g^{\text{f}} (v_0 - J^{\text{f}}_{\text{water}}) , \tag{S9}$$

$$P_*^{\text{b}} = P_0^{\text{b}} - d_g^{\text{b}} (v_0 + J^{\text{b}}_{\text{water}}) , \tag{S10}$$

where d_g is the coefficient of hydraulic resistance and is related to the viscosity and geometrical properties of the extracellular space (see later sections for derivations).

The velocity of the cell leading edge is also the result of membrane movement, which has two contributions: the translational velocity of the membrane, v_m, and the velocity from membrane trafficking, v_{tk}. v_m is the velocity of membrane in the lab frame. The surrounding extracellular matrix or channel walls exerts a frictional force on the membrane proportional to v_m and the cell length. v_{tk} is the movement of the cell leading edge due to vesicle trafficking from the back to the front of a cell because as more membrane is added from the back to the front, the cell membrane must extend forward. We thus have

$$v_0 = v_m + v_{\text{tk}} . \tag{S11}$$

In general, vesicle trafficking occurs at both ends of the cell, the difference of which determines v_{tk}, i.e., $v_{\text{tk}} = v_{\text{tk}}^{\text{b}} - v_{\text{tk}}^{\text{f}}$. The rate of vesicle trafficking should depend on membrane tension, τ. We approximate this rate as a linear function in τ such that when $\tau = 0$ the rate of trafficking reaches the maximum, γ_{tk}^0, and when the membrane tension reaches the maximum, τ_{max}, the trafficking stops. Therefore, v_{tk} can be written as

$$v_{\text{tk}} = \gamma_{\text{tk}}^0 \left(1 - \frac{\tau^{\text{b}}}{\tau_{\text{max}}} \right) - \gamma_{\text{tk}}^0 \left(1 - \frac{\tau^{\text{f}}}{\tau_{\text{max}}} \right) . \tag{S12}$$

The membrane tension at the two ends, $\tau^{\text{b/f}}$, is obtained through force balances, i.e.,

$$2\tau^{\text{f/b}} = b\left(P_{\text{in}}^{\text{f/b}} - P_{*}^{\text{f/b}}\right) + bf_{\text{ext}}^{\text{f/b}}\,, \tag{S13}$$

where P_{in} is the volume-weighted average intracellular pressure given by $P_{\text{in}} = \theta_c P_c + \theta_n P_n$, in which P_n is the effective pressure in the actin phase. f_{ext}, defined positive outwards the cell, is the sum of all the external applied or structural forces per unit area. These forces can come various reasons including applied bead attraction or repulsion.

In principle there is phase exchange between the cytosol phase and the F-actin phase because during actin polymerization and depolymerization, some of the volume of the cytosol, in the form of G-actin monomers, is converted to the actin network phase [3]. Since the volume fraction of G-actin monomers in the cytosol is very small compared to the overall cytosol volume fraction, this phase interchange can be neglected. At steady-state the volume conservation of the two phases are

$$\frac{d}{dx}(\theta_n v_n') = 0\,, \tag{S14}$$

$$\frac{d}{dx}(\theta_c v_c') = 0\,. \tag{S15}$$

The vanishing right hand sides is consistent with our modeling approximations that (i) there are no sink or source in the interior of the cell, (ii) J_{water} and J_{actin} only serve as boundary conditions for the two phases, and (iii) no inter-phase volume exchange occurs in the cell.

We now consider the force balance equations of the two phases. Since the viscosity of the cytosol is close to that of water and is small (10^{-3} Pa·s), the viscous effect within the cytosol phase is thus negligible. Depending on the geometry of the cell, the nucleus may restrict cytosol fluid flow. We model this restriction by adding additional friction terms when flow passes through the nucleus. We also consider the focal adhesion friction force between the actin network and the substrate, which is effectively a body force in the actin phase. The force balance can then be written as

$$0 = -\theta_c \frac{d}{dx}P_c + \eta\theta_n\theta_c(v_n' - v_c') - \zeta_c\theta_c v_c'\,, \tag{S16}$$

$$\begin{aligned} 0 = &-\theta_n \frac{d}{dx}P_c - \eta_n\theta_n[v_n' + (v_0 - v_m)] + \eta\theta_n\theta_c(v_c' - v_n') \\ &- \frac{d}{dx}(\theta_n\phi_n) - \eta_{\text{st}}\theta_n(v_n' + v_0) - \zeta_n\theta_n v_n'\,, \end{aligned} \tag{S17}$$

where η is the coefficient of inter-phase viscous drag. η_n is the effective viscosity of the actin phase. For a quadratic flow profile in z, $\eta_n = 12\mu_n/b^2$, where b is the width of the cell and μ_n is the dynamic viscosity of the actin phase, which is typically 10^3 times the viscosity of water [4]. The term $(v_0 - v_m)$ corrects the viscous force if there is any vesicle trafficking. The effective pressure in the actin phase can be written as $P_n = P_c + \phi_n$, where ϕ_n is the excess pressure in the actin network. This pressure comes from

expansion/contraction of the actin gel and myosin contraction. η_{st} is the coefficient of focal adhesion force between the actin dynamics and the external matrix of the cell. The force from focal adhesion is proportional to the absolute velocity of the actin network, $v_n = v_n' + v_0$, when the network velocity is low [5]. $\zeta_c(x)$ and $\zeta_n(x)$ are the coefficients of frictional drag from the nucleus on the cytosol and actin phases, respectively; these are only defined in the region of the nucleus.

With all the forces considered, we can write the force balance on the entire cell membrane as

$$b\left[\left(P_{\text{in}}^{\text{f}} - P_*^{\text{f}}\right) - \left(P_{\text{in}}^{\text{b}} - P_*^{\text{b}}\right)\right] = -b\eta_n \int_0^L \theta_n[v_n' + (v_0 - v_m)]dx + 2\xi_m v_m L - bf_{\text{ext}}^{\text{f}} + bf_{\text{ext}}^{\text{b}}\,. \quad \text{(S18)}$$

On the right hand side of Eq. S18, the first term is the viscous drag on the lateral membrane from the actin network. The second term is the frictional drag between the cell membrane and the surroundings, where ξ_m is the drag coefficient. In both terms we count for two surfaces $z = 0$ and $z = b$ as shown in Fig. S1A. The exact drag may vary depending on the geometry; for example, a strip of a cell on 2D may only experience frictional drag at the lower surface. This difference does not qualitatively change the results of the model, and we will keep the two terms in the current form.

In this system of equations, we have six unknowns: P_c, v_c', v_n', θ_n, v_0, and v_m. The the six equations to solve the unknowns are Eqs. S14, S15, S16, S17, S11, and S18. Equations S14, S15, S16, and S17 are four first-order differential equations and the four boundary conditions come from Eqs. S1, S4, S6, and S7.

Here we make a few notes on this system. Adding Eq. S16 to Eq. S17 and using Eqs. S9 and S10 rewrites Eq. S18 as

$$\begin{aligned} &- b\int_0^L (\zeta_c\theta_c v_c' + \zeta_n\theta_n v_n')dx - b\eta_{\text{st}}\int_0^L \theta_n(v_n' + v_0)dx \\ &= 2\xi_m v_m L + bd_g\left(v_0 - J_{\text{water}}\right) - bf_{\text{ext}}^{\text{f}} + bf_{\text{ext}}^{\text{b}}\,, \end{aligned} \quad \text{(S19)}$$

where we have used $P_0^{\text{f}} = P_0^{\text{b}}$ and $d_g = d_g^{\text{f}} + d_g^{\text{b}}$ (see below). With Eqs. S1, S7, and S14, Eq. S19 can be simplified as

$$\begin{aligned} &bL_\zeta(\zeta_c J_{\text{water}} + \zeta_n J_{\text{actin}}) + bL\eta_{\text{st}}(J_{\text{actin}} - \Theta_n v_0) \\ &= 2\xi_m v_m L + bd_g\left(v_0 - J_{\text{water}}\right) - bf_{\text{ext}}^{\text{f}} + bf_{\text{ext}}^{\text{b}}\,. \end{aligned} \quad \text{(S20)}$$

Here we can clearly see the dominant contributions to the velocity of the cell leading edge. In the limit of $v_m = v_0$, the velocity v_0 can be expressed as

$$v_0 = \frac{L_\zeta(\zeta_c J_{\text{water}} + \zeta_n J_{\text{actin}}) + L\eta_{\text{st}} J_{\text{actin}} + d_g J_{\text{water}} + f_{\text{ext}}^{\text{f}} - f_{\text{ext}}^{\text{b}}}{L\eta_{\text{st}}\Theta_n + 2\xi_m L/b + d_g}\,. \quad \text{(S21)}$$

These simple expressions provide an easy way to estimate the order of magnitude of contribution from each physical quantities. We will explore the quantities in more detail in the later sections and also in the main text.

1.1 Approximate d_g in 1D and 2D

The hydraulic resistance experienced by a cell is also the extracellular pressure on the cell. The motion of the extracellular fluid is governed by Stokes flow,

$$0 = -\nabla P_* + \mu_f \nabla^2 \mathbf{v}_* \,, \tag{S22}$$

where μ_f is the extracellular fluid viscosity and the subscript '*' denotes the extracellular space. The Laplacian term is on the order of $\mathbf{v}_*/\lambda^2$, where λ is the characteristic length scale of the extracellular space.

For cells in 1D channels, d_g can be solved explicitly. Let ℓ_0 be the total length of a 1D channel and denote ℓ_0^{b} and ℓ_0^{f} as the extracellular fluid length in the channel behind and in front of the cell, respectively (see Fig. S1C). In most cases $L \ll \ell_0$ so that $\ell_0^{\mathrm{b}} + \ell_0^{\mathrm{f}} \simeq \ell_0$. As an example, we solve the fluid field at the front side of the cell. Since the flow is only one-dimensional, we let v_* be the height-averaged $x-$component of $\mathbf{v}_*$. From the Stoke's equation we have

$$v_*(z) = \frac{1}{2\mu_f}\frac{\partial P_*}{\partial x}(z^2 - bz) \,. \tag{S23}$$

Then the cross-sectional averaged velocity of v_* is

$$\bar{v}_* = \frac{1}{b}\int_0^b v_*(z)dz = -\frac{b^2}{12\mu_f}\frac{\partial P_*}{\partial x} \,. \tag{S24}$$

Since $\bar{v}_* = v_0 - J^{\mathrm{f}}_{\mathrm{water}}$, we can write

$$P_*^{\mathrm{f}} - P_0^{\mathrm{f}} = \frac{12\mu_f \ell_0^{\mathrm{f}}}{b^2}(v_0 - J^{\mathrm{f}}_{\mathrm{water}}) \,. \tag{S25}$$

Comparing Eqs. S25 with S9, the coefficient of hydraulic resistance at the front is given by $d_g^{\mathrm{f}} = 12\mu_f \ell_0^{\mathrm{f}}/b^2$. Similarly, the coefficient of hydraulic resistance at the back is $d_g^{\mathrm{b}} = 12\mu_f \ell_0^{\mathrm{b}}/b^2$. The total hydraulic resistance on the cell is the combined effect of the pressure at the front and the back. Hence, the net coefficient of hydraulic resistance for a 1D channel is $d_g^{\mathrm{1D}} = d_g^{\mathrm{b}} + d_g^{\mathrm{f}} = 12\mu_f \ell_0/b^2$. When, for example, $b = 5$ μm, $\ell_0 = 500$ μm, and $\mu_f = 10^{-3}$ Pa·s, then d_g is about 2.5×10^{-1} Pa·s/μm. If the viscosity or length of the extracellular fluid increases, d_g^{1D} will scale accordingly.

Eq. S25 shows that the characteristic length scale of a 1D channel is b, the width of the channel. For cells migrating on a 2D substrate, the extracellular space is infinite compared to the size of the cell and thus the pressure difference across the extracellular space is negligible. As an approximation, we thus let $d_g^{\mathrm{2D}} \simeq 0$ in this study.

For comparison, when a sphere of radius b is placed in a flow of viscosity μ_f, the viscous drag acting on the sphere is $6\pi\mu_f b u$, where u is the velocity of the flow [6]. Based on our definition of the coefficient of hydraulic resistance, the effective d_g in this case is $6\mu_f/b$, which is $2\ell_0/b$ times smaller than the hydraulic resistance coefficient in a 1D channel.

1.2 Effect of d_g on J_{water}

Eq. S8 shows that the water flux depends on the external fluid pressure, P_*, and thus on the coefficient of hydraulic resistance, d_g. Here we discuss the effect of d_g on J_{water}. Let us take the front end of the cell as an example. Substituting Eq. S9 into Eq. S8 yields

$$J^{\text{f}}_{\text{water}} = -\frac{\alpha^{\text{f}}}{1+\alpha^{\text{f}} d^{\text{f}}_g}\left[(P^{\text{f}}_c - P^{\text{f}}_0) - RT(c^{\text{f}}_{\text{in}} - c^{\text{f}}_{\text{in}})\right] + \frac{\alpha^{\text{f}} d^{\text{f}}_g}{1+\alpha^{\text{f}} d^{\text{f}}_g} v_0\,. \tag{S26}$$

Since $d^{\text{f}}_g + d^{\text{b}}_g = d_g$, then $d^{\text{f}}_g < d_g$ is always true. Without loss of generality, we may let $d^{\text{f}}_g = d_g/2$. When d^{f}_g is small such as $d^{\text{f}}_g = 10^2$ Pa·s/μm, then $\alpha^{\text{f}} d^{\text{f}}_g \ll 1$ given that α^{f} is around 10^{-6} μm/(Pa·s) (Tab. **??**). The cell boundary velocity v_0 is on the order of 10 nm/s so that $d^{\text{f}}_g v_0 \sim 1$ Pa, which is much smaller than P_c. Hence, Eq. S26 is reduced to

$$J^{\text{f}}_{\text{water}} = -\alpha^{\text{f}}\left[(P^{\text{f}}_c - P^{\text{f}}_0) - RT(c^{\text{f}}_{\text{in}} - c^{\text{f}}_{\text{in}})\right]\,, \tag{S27}$$

which is the same as the case without considering the hydraulic resistance. On the other hand, when d^{f}_g is large such as $d^{\text{f}}_g = 10^6$ Pa·s/μm, then $d^{\text{f}}_g v_0 \sim 10^4$ Pa, which is much larger than P_c. The ratio $\alpha^{\text{f}} d^{\text{f}}_g/(1+\alpha^{\text{f}} d^{\text{f}}_g)$ approaches to 1 when $\alpha^{\text{f}} d^{\text{f}}_g \gg 1$. Hence, $J^{\text{f}}_{\text{water}} = v_0$ for large d^f_g; this is consistent with the approximated expression of v_0 in Eq. S21 as d_g approaches to infinity, i.e.,

$$\lim_{d_g \to \infty} v_0 = J_{\text{water}}\,. \tag{S28}$$

Similarly, at the back of the cell the water flux is expressed as

$$J^{\text{b}}_{\text{water}} = -\frac{\alpha^{\text{b}}}{1+\alpha^{\text{b}} d^{\text{b}}_g}\left[(P^{\text{b}}_c - P^{\text{b}}_0) - RT(c^{\text{b}}_{\text{in}} - c^{\text{b}}_{\text{in}})\right] - \frac{\alpha^{\text{b}} d^{\text{b}}_g}{1+\alpha^{\text{b}} d^{\text{b}}_g} v_0\,, \tag{S29}$$

and the similar conclusion is drawn.

1.3 Approximate d_g in 3D

For cells in 3D collagen matrix, we consider the resistance at the front of cell protrusions as the protrusions, which are effectively 1D structures, extend in space. We approximate a long protrusion as a sphero-cylinder with radius r_0 (see Fig. 4A in the main text). Let θ_* be the porosity of the collagen matrix. The force balance of the cell membrane at the front of the protrusion is

$$2\tau^{\text{f}} = r_0\left(P^{\text{f}}_{\text{in}} - \sigma^{\text{f}}_*\right) + r_0 f^{\text{f}}_{\text{ext}}\,, \tag{S30}$$

where σ^{f}_* is the effective pressure of the matrix at the front of the protrusion,

$$\sigma^{\text{f}}_* = \theta_* P^{\text{f}}_* + (1-\theta_*) P^{\text{f}}_{\text{col}}\,, \tag{S31}$$

where P^{f}_* is the fluid pressure in the pores and $P^{\text{f}}_{\text{col}}$ is the pressure from the collagen fibers, both evaluated at the front of the protrusion. $\theta_* P^{\text{f}}_*$ is the hydraulic resistance to the protrusion. The combination of $(1-\theta_*)P^{\text{f}}_{\text{col}}$

and $f_{\text{ext}}^{\text{f}}$ can be regarded as the total external force at the front of the protrusion. The pressure, P_{col}, in the collagen fibers comes from cell protrusion, which deforms the collagen and introduces a stress field within the collagen. The collagen matrix is a nonlinear, viscoelastic, porous material exhibiting strain-stiffening [7] and stress relaxation [8]. The collagen fiber alignment, matrix pore size, and the expression of the matrix metalloproteinases on the cell protrusion [9] all affect the interaction between the cell protrusion and the collagen matrix, and thus the pressure P_{col}. In this work, we are primarily interested in approximating the coefficient of hydraulic resistance in 3D collagen matrix and comparing it to the coefficients in 1D and 2D; we will therefore not solve P_{col} in detail.

Due to high porosity of the collagen hydrogel matrix and the fact that cells can actively cut collagen fibers, we can approximate the fluid pressure in the pores by solving the uncoupled consolidation equation

$$\frac{\partial P_*}{\partial t} - c\nabla^2 P_* = 0\,, \tag{S32}$$

where c is the coefficient of consolidation.

The cell front protrudes at velocity v_0, which acts as a continuous pressure source in space and time that pushes the fluid in the collagen matrix. To simplify the matter, we may focus on each instantaneous moment where the pressure source is spatially fixed. In this case, the pressure source at the front of the protrusion can be considered as a Dirac delta function in time with the amplitude P_*^{f} that serves as a boundary condition for the pore pressure in the matrix. Since the dimension of the protrusion is much smaller than that of the collagen matrix, we may assume that the existence of the protrusion does not significantly influence the pressure field in space and the pressure field propagates freely in the matrix. In this case, the pressure field radiated from the tip of the protrusion is spherically symmetric, i.e.,

$$\frac{1}{r^2}\frac{\partial}{\partial r}\left(r^2\frac{\partial P_*}{\partial r}\right) - \frac{1}{c}\frac{\partial P_*}{\partial t} = 0\,, \tag{S33}$$

which can be rewritten as

$$\frac{\partial^2}{\partial r^2}\left(rP_*\right) - \frac{1}{c}\frac{\partial}{\partial t}(rP_*) = 0\,. \tag{S34}$$

The consolidation equation is best solved in the frequency domain with a harmonic time form of the solution, i.e., $P_* = \tilde{P}_* \exp(i\omega t)$, where the tilde denotes a quantity in the frequency domain. Eq. S34 then becomes

$$\frac{\partial^2}{\partial r^2}\left(r\tilde{P}_*\right) - \frac{i\omega}{c}(r\tilde{P}_*) = 0\,. \tag{S35}$$

An infinite domain implies that there is no wave reflection. Therefore, the solution to Eq. S35 is

$$\tilde{P}_* = \tilde{P}_*^{\text{f}}\frac{r_0}{r}e^{\sqrt{\frac{i\omega}{c}}(r_0-r)} = \tilde{P}_*^{\text{f}}\frac{r_0}{r}e^{\sqrt{\frac{\omega}{2c}}(1+i)(r_0-r)}\,, \tag{S36}$$

where $\tilde{P}_*^{\text{f}}$ is the pore pressure at the front of the cell associated with frequency ω. $\tilde{P}_*^{\text{f}}$ and P_*^{f} have the same value in number since the pressure source is a delta function in time. From the decay rate in Eq. S36, the length scale of the pressure wave propagation is $L_p = \sqrt{2c/\omega}$, which decreases with increasing frequency.

The fluid flow in the porous collagen matrix follows Darcy's Law, i.e.,

$$0 = -\nabla P_* - \frac{\mu_f}{\kappa}\mathbf{v}_* \,, \tag{S37}$$

where κ is the permeability of the collagen matrix. In the spherical coordinate the fluid velocity can be solved as

$$v_* = -\frac{\kappa}{\mu_f}\frac{\partial P_*}{\partial r} \,. \tag{S38}$$

The boundary condition of the velocity is

$$v_*\big|_{r=r_0} = -\frac{\kappa}{\mu_f}\frac{\partial P_*}{\partial r}\big|_{r=r_0} = v_0 - J^{\rm f}_{\rm water} \,, \tag{S39}$$

which can also be written in the frequency domain. The combination of Eqs. S36 and S39 yields

$$\tilde{v}^{\rm f}_* = \tilde{v}_0 - \tilde{J}^{\rm f}_{\rm water} = \frac{\mu_f}{\kappa}\left[\frac{1}{r_0} + \sqrt{\frac{\omega}{2c}}(1+i)\right]^{-1} \tilde{P}^{\rm f}_* \,. \tag{S40}$$

Equation S40 gives the coefficient of hydraulic pressure in the frequency domain

$$\tilde{d}_g = \frac{\mu_f}{\kappa}\left[\frac{1}{r_0} + \sqrt{\frac{\omega}{2c}}(1+i)\right]^{-1} \,. \tag{S41}$$

The dominant ones are those of low frequencies. Indeed, as seen in Eq. S36, components of high frequencies are unable to propagate through long distance. On the first order of approximation, the coefficient of hydraulic resistance in 3D collagen matrix is $d_g^{\rm 3D} = \mu_f r_0/\kappa$, which is equivalent to assuming that the fluid in the pore is incompressible such that the consolidation equation (Eq. S32) is replaced by $\nabla^2 P_* = 0$. Thus, the coefficient of hydraulic resistance in a 3D collagen matrix depends on the permeability, and thus the pore size, of the matrix.

2 Supplementary Figures

References

[1] K. M. Stroka, H. Jiang, S.-H. Chen, Z. Tong, D. Wirtz, S. X. Sun, and K. Konstantopoulos. Water permeation drives tumor cell migration in confined microenvironments. *Cell*, 157:611–623, 2014.

[2] Y. Li, Y. Mori, and S. X. Sun. Flow-driven cell migration under external electric fields. *Phys. Rev. Lett.*, 115:268101, 2015.

[3] I. R. Kuznetsov, M. Herant, and M. Dembo. Analysis of actin FLAP dynamics in the leading lamella. *PLOS One*, 5(4):e10082, 2010.

[4] D. Wirtz. Particle-tracking microrheology of living cells: principles and applications. *Annu. Rev. Biophys.*, 38:301–326, 2009.

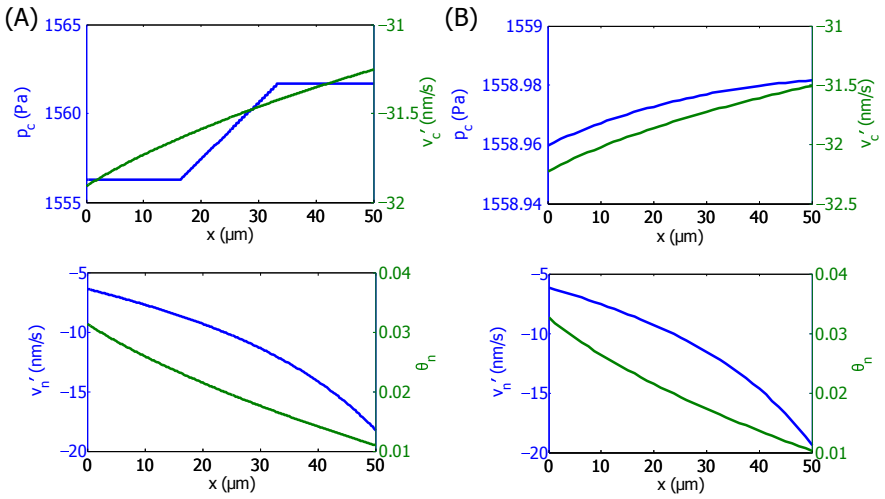

Figure S2: **Nucleus increases the intracellular pressure gradient.** Distribution of the intracellular hydrostatic pressure and cytosol velocity with respect to the cell frame, actin velocity with respect to the cell frame, and the volume fraction of the actin phase.(A) Prediction with drags from the nucleus. The predicted water flux and cell velocity are $J_{\text{water}} = 30.90$ nm/s, $v_0 = v_m = 12.38$ nm/s. (B) Prediction without drags from the nucleus. The predicted water flux and cell velocity are $J_{\text{water}} = 31.18$ nm/s, $v_0 = v_m = 11.89$ nm/s.

[5] M. L. Gardel, B. Sabass, L. Ji, G. Danuser, U. S. Schwarz, and C. M. Waterman. Traction stress in focal adhesions correlates biphasically with actin retrograde flow speed. *J. Cell. Biol.*, 183(6):999–1005, 2008.

[6] T. E. Faber. *Fluid dynamics for physicists*. Cambridge University Press, New Yorkm NY., 1995.

[7] A. M. Stein, D. A. Vader, D. A. Weitz, and L. M. Sander. The micromechanics of three-dimensional collagen-i gels. *Complexity*, 16(4):22–28, 2011.

[8] S. Nam, K. H. Hu, M. J. Butte, and O. Chaudhuri. Strain-enhanced stress relaxation impacts nonlinear elasticity in collagen gels. *Proc. Natl. Acad. Sci.*, 113(20):5492–5497, 2016.

[9] S. I. Fraley, P. H. Wu, L. He, Y. Feng, R. Krisnamurthy, G. D. Longmore, and D. Wirtz. Three-dimensional matrix fiber alignment modulates cell migration and MT1-MMP utility by spatially and temporally directing protrusions. *Sci. Rep.*, 5:14580, 2015.

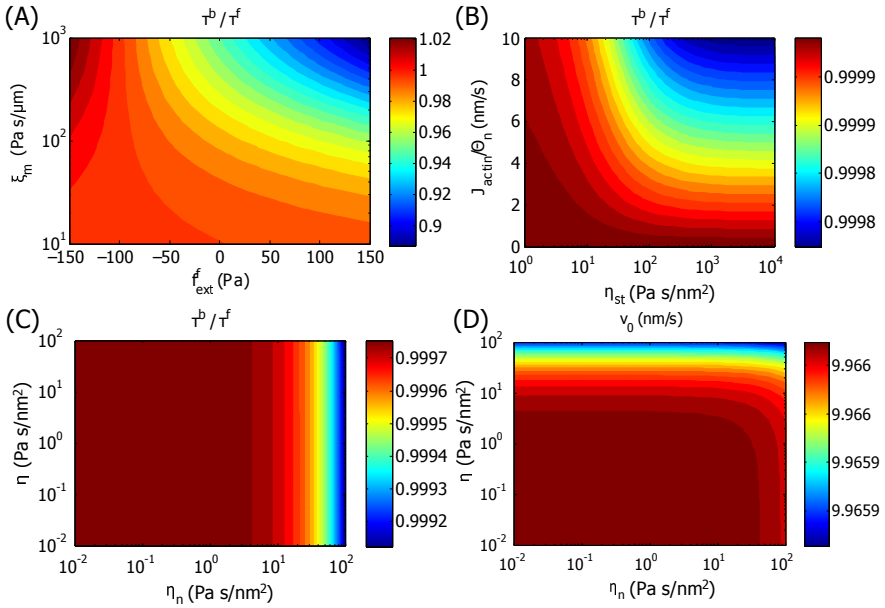

Figure S3: (A) Contour of the ratio of membrane tension at the back to the front, τ^{b}/τ_f, as ξ_m and $f^{\mathrm{f}}_{\mathrm{ext}}$ vary. The tension difference across the cell can be up to 10% under some friction on the channel wall and the external forces. (B) Contour of the ratio of membrane tension at the back to the front, τ^{b}/τ_f, as J_{actin} and η_{st} vary. (C) Contour of the ratio of membrane tension at the back to the front, τ^{b}/τ_f, as η and η_n vary. From (B) and (C) we can see that large variation of J_{actin}, η_{st}, η, or η_n does not lead to a non-uniform distribution of the membrane tension. (D) Contour of the v_0 as η and η_n vary. We can see that v_0 does not vary with η or η_n.

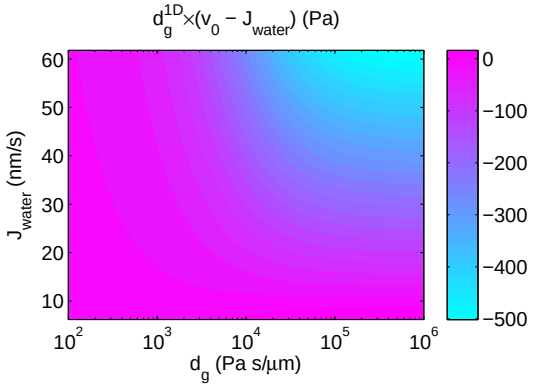

Figure S4: Effective hydraulic resistance experienced by a cell as J_{water} and d_g^{1D} vary. When a cell migrates in a confined channel, the effective hydraulic resistance experienced by the cell can be computed from $d_g^{\text{1D}}(v_0 - J_{\text{water}})$. Note that as v_0 increases towards the velocity of water flux, the difference, $v_0 - J_{\text{water}}$, reduces accordingly. Although the coefficient of hydraulic resistance has varied over four orders of magnitudes from 10^2 to 10^6 Ps·s/μm, the actual hydraulic resistance remains in the same order of magnitude. This shows that the cell increases its velocity to reduce the hydraulic resistance which would otherwise increase by several orders of magnitude.